Energy levels and Wavefunctions of the Hulthén Potential
Physics 214 Final Project

Harrison West, Majdouline Benlahcen, Patrick Wang, Josh Brown, Aidan Lacy, and Jack Bonner

Haverford College Department of Physics and Astronomy

(Dated: April, 2025)

The Hulthén potential is a useful model for many quantum mechanical systems. In conjunction with the finite difference method to solve the time-independent Schrödinger equation, we use a discretized approximation of this potential to obtain allowed system energies and their corresponding wavefunctions. We compare our results with simulated and calculated results from previously published literature. We also explore how system behavior including number of allowed energy levels and lowest allowed energy level vary when system parameters are changed.

I. INTRODUCTION

The Hulthén potential behaves similarly to a screened Coulomb potential at sufficiently small distances. As such, it is a strong mathematical basis from which we can explore a wide range of nuclear, atomic, chemical, and solid-state physical systems. For example, the Hulthén potential models the shape-invariant supersymmetry of diatomic molecules (Jia et al. [2]); the enclosure of an atom within a spherically impenetrable box (Roy [4]); and the interaction between the nucleons in the nucleus of a deuterium atom (Bhoi and Laha [1]).

The Hulthén potential is given by

$$V(r) = -Z\delta e^{-\delta r}/(1 - e^{-\delta r}) \quad (1)$$

When used to model an atom, Z is given by the atomic number (Varshni [5]). As in Varshni [5], we set $Z \equiv 1$ to model a Hydrogen atom. The screening parameter δ indicates the degree to which the effective electric field experienced by a charge is weakened due to the presence of other charged particles. In this paper, we use the Hulthén potential's boundary conditions and the finite-difference method to evaluate the following:

1. The total number of energy states of the system, their energy levels, and their corresponding (radial) wavefunctions

2. The uncertainties of the radius and momentum; and product of the two uncertainties; and how each of the three values changes with the system's energy level

II. METHODS

The Time-Independent Schrödinger Equation (TISE) for a particle in a spherically symmetric potential is given by:

$$-\frac{\hbar^2}{2m}\nabla^2\psi(r,\theta,\phi) + V(r)\psi(r,\theta,\phi) = E\psi(r,\theta,\phi)$$

where ∇^2 is the Laplacian, and $\psi(r,\theta,\phi)$ is the wavefunction in terms of spherical coordinates.

The Laplacian, in spherical coordinates, is given by:

$$\nabla^2 = \frac{1}{r^2}\frac{\partial}{\partial r}\left(r^2\frac{\partial}{\partial r}\right) + \frac{1}{r^2\sin\theta}\frac{\partial}{\partial\theta}\left(\sin\theta\frac{\partial}{\partial\theta}\right) + \frac{1}{r^2\sin^2\theta}\frac{\partial^2}{\partial\phi^2}$$

Next, we apply a separation of variables, only possible because we assumed the wavefunction can be written as the product of radial and angular functions:

$$\psi(r,\theta,\phi) = R_\ell(r)Y_{\ell,m}(\theta,\phi)$$

Substituting the separation of variables into the Schrödinger equation yields:

$$-\frac{\hbar^2}{2m}\left[\frac{1}{r^2}\frac{d}{dr}\left(r^2\frac{d}{dr}[R_\ell(r)Y_{\ell,m}(\theta,\phi)]\right) + \frac{\ell(\ell+1)}{r^2}[R_\ell(r)Y_{\ell,m}(\theta,\phi)]\right] + V(r)[R_\ell(r)Y_{\ell,m}(\theta,\phi)]$$
$$= E[R_\ell(r)Y_{\ell,m}(\theta,\phi)]$$

This equation can be separated into two parts, corresponding to the radial and angular components. The latter satisfies the spherical harmonics equation:

$$\frac{1}{\sin\theta}\frac{\partial}{\partial\theta}\left(\sin\theta\frac{\partial Y_{\ell,m}(\theta,\phi)}{\partial\theta}\right) + \frac{1}{\sin^2\theta}\frac{\partial^2 Y_{\ell,m}(\theta,\phi)}{\partial\phi^2}$$
$$= -\ell(\ell+1)Y_{\ell,m}(\theta,\phi)$$

The solutions to this equation are the well studied spherical harmonics $Y_{\ell,m}(\theta,\phi)$, which have the form:

$$Y_{\ell,m}(\theta,\phi) = N_{\ell,m}P_{\ell,m}(\cos\theta)e^{im\phi}$$

where $P_{\ell,m}(\cos\theta)$ are the associated Legendre polynomials and $N_{\ell,m}$ is a normalization factor.

The radial component of the Schrödinger equation then becomes:

$$-\frac{\hbar^2}{2m}\left[\frac{1}{r^2}\frac{d}{dr}\left(r^2\frac{dR_\ell(r)}{dr}\right) - \frac{\ell(\ell+1)}{r^2}R_\ell(r)\right]$$
$$+ V(r)R_\ell(r) = ER_\ell(r)$$

We cast the equation into atomic units, where

$$\hbar = m = e = 1$$

This generates the Hulthén potential threshold condition given by Patil [3], where the radial wavefunction $R_\ell(r)$ satisfies the equation

$$-\frac{1}{2}\left[\frac{1}{r}\frac{d^2}{dr^2}r - \frac{\ell(\ell+1)}{r^2}\right]R_\ell(r) + V(r)R_\ell(r)$$
$$= ER_\ell(r) \quad (2)$$

where as before, $V(r)$ is the Hulthén potential, and ℓ is the orbital quantum number. We choose $\ell > 0$ to exclude the s orbitals.

Here we define the radial wavefunction as is standard to do:

$$U(r) \equiv rR_\ell(r)$$

hence Equation 2 can be rewritten as

$$-\frac{1}{2}\frac{d^2U(r)}{dr^2} + \frac{\ell(\ell+1)}{2r^2}U(r) + V(r)U(r) = EU(r) \quad (3)$$

By the finite difference method,

$$\frac{d^2U(r)}{dr^2} \approx \frac{U(r+\Delta r) - 2U(r) + U(r-\Delta r)}{\Delta r^2}$$

When discretized such that $r_j \equiv j\Delta r$ and $U(r_j) \equiv U_j$ for non-negative integer values of j, the second derivative of U is approximated by

$$\frac{d^2U_j}{dr^2} \approx \frac{U_{j+1} - 2U_j + U_{j-1}}{\Delta r^2} \quad (4)$$

Substituting Equation 4 into Equation 3, therefore, yields the relation

$$U_j\left[\frac{1}{\Delta r^2} + \frac{\ell(\ell+1)}{2(j\Delta r)^2} + V_j\right]$$
$$+ U_{j-1}\left[\frac{-1}{2\Delta r^2}\right] + U_{j+1}\left[\frac{-1}{2\Delta r^2}\right] = EU_j \quad (5)$$

Treating Equation 5 as an eigenvalue equation, we equate it to the tri-diagonal Hamiltonian matrix

$$[H]_{ij} = \begin{cases} \frac{1}{\Delta r^2} - \frac{Z\delta e^{-\delta j\Delta r}}{1-e^{-\delta j\Delta r}} + \frac{\ell(\ell+1)}{(j\Delta r)^2}, & i = j \\ -\frac{1}{2\Delta r^2}, & i = j \pm 1 \\ 0, & \text{otherwise} \end{cases} \quad (6)$$

The eigenvalue-eigenvector pairs of this matrix, designated E_s and $\vec{v}_s$ for a given state s, correspond to the Energy levels and their wavefunctions as approximated by equally spaced nodes along the r axis. We note that this matrix will have a number of solutions equal to it's dimensions, and identify the physically allowed solutions as only those with Eigen-energy $E_s < 0$, which indicates that the modeled electron is in a bound state.

To normalize the wavefunction approximations, we square the wavefunction solutions to Equation 6, and approximate the integral of this function with the composite trapezoidal rule:

For a discrete function $f(x)$ with n equally spaced points between a and b, those points are labeled x_i where $i = 1,2,3,\ldots,n$. If we define

$$x_0 = a; x_{n+1} = b; \Delta x = \frac{b-a}{n+1}$$

then the integral of that discrete function is approximated by

$$\int_a^b f(x)dx \approx \Delta x\left[\frac{f(x_{n+1}) + f(x_0)}{2} + \sum_{k=1}^n f(x_k)\right] \quad (7)$$

We treat the vector $\vec{v}_s$ as a discrete function $v_s(r)$ such that the approximate wavefunction of a given state s is given by

$$v_s(r) = \begin{bmatrix} v_{s,1} \\ v_{s,2} \\ \vdots \\ v_{s,N} \end{bmatrix}; \quad v_s^2(r) = \begin{bmatrix} v_{s,1}^2 \\ v_{s,2}^2 \\ \vdots \\ v_{s,N}^2 \end{bmatrix}$$

and approximate the integral

$$\int_{r=0}^q v_s^2(r)dr$$

Where q is an arbitrarily large radius such that

$$v(q) \to 0$$

The composite trapezoidal rule estimates for the area under the "curve" of the squared wavefunction approximation. Based on our definition of $v_s(r)$ if

$$\int_a^b v_s^2(r)dr = C$$

then the normalized wavefunction approximation is given by

$$\mathrm{v}_s(r) = \frac{1}{\sqrt{C}}v_s(r)$$

The uncertainty of an observable A is given by

$$\Delta A = \sqrt{\langle A^2 \rangle - \langle A \rangle^2}$$

We seek expressions for the radial operator and its square, and the radial components of both the momentum operator and its square.

The radial operators are given by

$$\hat{r} = r; \quad \hat{r}^2 = r^2$$

The momentum operator in this case is the spherical-coordinate gradient, which has radial component

$$\hat{p}_r = -i\hbar \frac{\partial}{\partial r}$$

The square of the gradient operator is the Laplace operator, so the radial component of the squared momentum operator is simply the radial component of the Laplace operator. This is given by:

$$\hat{p}_r^2 = -\hbar^2 \frac{1}{r^2} \frac{\partial}{\partial r} \left(r^2 \frac{\partial}{\partial r} \right)$$

Recall that from our usage of atomic units, the factor of $\hbar$ will vanish from both operators. Since the wavefunctions are real, we replace their complex conjugates with themselves, so the expectation values of these operators are given by

$$\langle A \rangle = \int_0^{R_{\max}} R_\ell(r) \hat{A} R_\ell(r) r^2 dr$$

Where the r^2 factor is added to account for the volumetric aspect of integrating a radial wavefunction.

Therefore, we find the radial expectation values as

$$\langle r \rangle = \int_0^{R_{\max}} R_\ell(r) r R_\ell(r) r^2 dr = \int_0^{R_{\max}} r U^2(r) dr$$

And similarly,

$$\langle r^2 \rangle = \int_0^{R_{\max}} r^2 U^2(r) dr$$

We also find

$$\langle p_r \rangle = \int_0^{R_{\max}} R_\ell(r) \left(-i \frac{\partial}{\partial r} \right) R_\ell(r) r^2 dr$$

$$= -i \int_0^{R_{\max}} r R_\ell(r) \cdot r \frac{\partial R_\ell(r)}{\partial r} dr$$

$$= -i \int_0^{R_{\max}} U(r) \cdot r \frac{\partial R_\ell(r)}{\partial r} dr$$

$$\langle p_r^2 \rangle = \int_0^{R_{\max}} R_\ell(r) \left(-\frac{1}{r^2} \frac{\partial}{\partial r} \left(r^2 \frac{\partial}{\partial r} \right) \right) R_\ell(r) r^2 dr$$

$$= - \int_0^{R_{\max}} R_\ell(r) \frac{\partial}{\partial r} \left(r^2 \frac{\partial R_\ell(r)}{\partial r} \right) dr$$

In our results, we use these values to calculate Δr, Δp, and $\Delta r \Delta p$ for the first four $\ell = 1$ energy levels.

III. RESULTS

TABLE I. Energies as eigenvalues of the Hamiltonian matrix (Equation 6) from this work compared to Varshni [5]. A negative sign before the energy has been omitted everywhere.

| State	δ	This Paper	Varshni Numerical	Varshni Analytical
2p	0.025	0.1127623	0.1127605	0.1127605
	0.05	0.1010443	0.1010425	0.1010425
	0.075	0.0898495	0.0898478	0.0898478
	0.1	0.0791812	0.0791794	0.0791794
	0.15	0.0594431	0.0594415	0.0594415
	0.2	0.0418875	0.0418860	0.0418860
	0.25	0.0266123	0.0266111	0.0266108
	0.3	0.0137910	0.0137900	0.0137878
	0.35	0.0037938	0.0037931	0.0037734
3p	0.025	0.0437077	0.0437069	0.0437069
	0.05	0.0331653	0.0331645	0.0331645
	0.075	0.0239405	0.0239397	0.0239397
	0.1	0.0160544	0.0160537	0.0160537
	0.15	0.0044667	0.0044663	0.0044660
3d	0.025	0.0436031	0.0436030	0.0436030
	0.05	0.0327533	0.0327532	0.0327532
	0.075	0.0230308	0.0230307	0.0230307
	0.1	0.0144848	0.0144842	0.0144842
	0.15	0.0013961	0.0013966	0.0013894
4p	0.025	0.0199493	0.0199489	0.0199489
	0.05	0.0110585	0.0110582	0.0110582
	0.075	0.0046210	0.0046219	0.0046219
	0.1	0.0007036	0.0007550	0.0007532
4d	0.025	0.0198463	0.0198462	0.0198462
	0.05	0.0106674	0.0106674	0.0106674
	0.075	0.0038336	0.0038345	0.0038344
4f	0.025	0.0196911	0.0196911	0.0196911
	0.05	0.0100620	0.0100620	0.0100620
	0.075	0.0025556	0.0025563	0.0025557
5p	0.025	0.0093929	0.0094036	
	0.05	0.0025532	0.0026490	
5d	0.025	0.0092969	0.0093037	
	0.05	0.0022357	0.0023131	
5f	0.025	0.0091491	0.0091521	
	0.05	0.0017305	0.0017835	
5g	0.025	0.0089458	0.0089465	
	0.05	0.0009898	0.0010159	
6p	0.025	0.0034646	0.0041548	
6d	0.025	0.0035103	0.0040606	
6f	0.025	0.0035420	0.0039168	
6g	0.025	0.0035200	0.0037201	
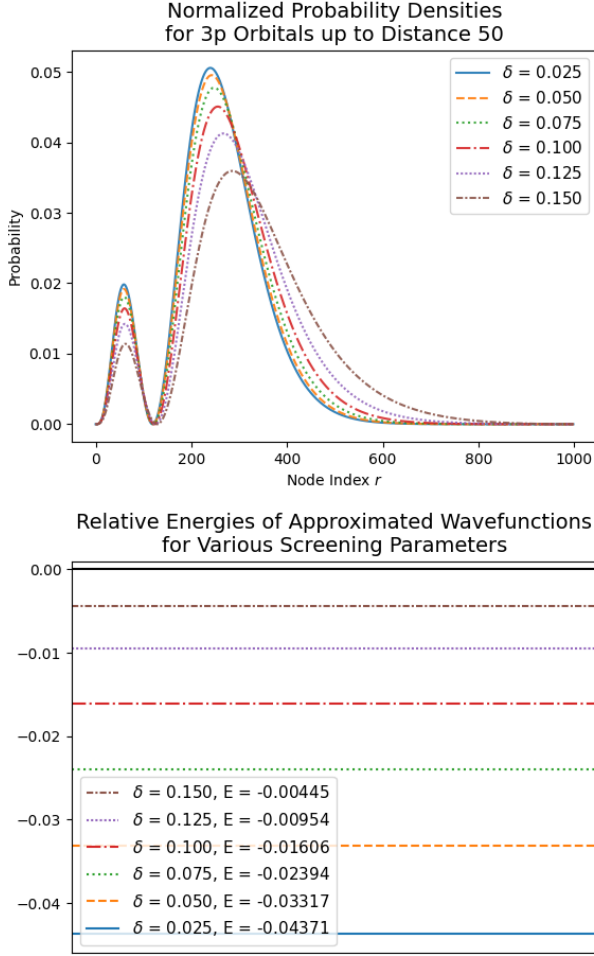
FIG. 1. Computed solutions for 6 values of δ in the 3p orbital ($n = 3, \ell = 1$) with 999 nodes over a radius of 50 a.u. Panel 1 shows the probability densities derived from the wavefunction eigenvectors. Panel 2 shows the energy level eigenvalues corresponding to each wavefunction. Linestyles and colors are matched to indicate correspondence.
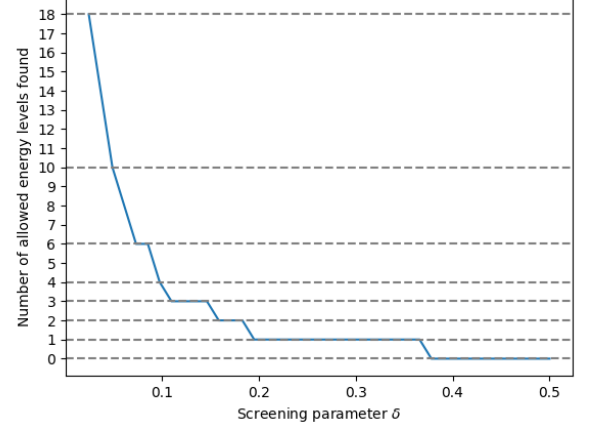

FIG. 2. Number of electron configurations with $E < 0$, for all $1 \leq \ell \leq 4$. We find occupancy in all states shown in Table I as well as 7p, 7d, 7f, and 7g, which accounts for this plot exceeding the number of states seen in Table I.
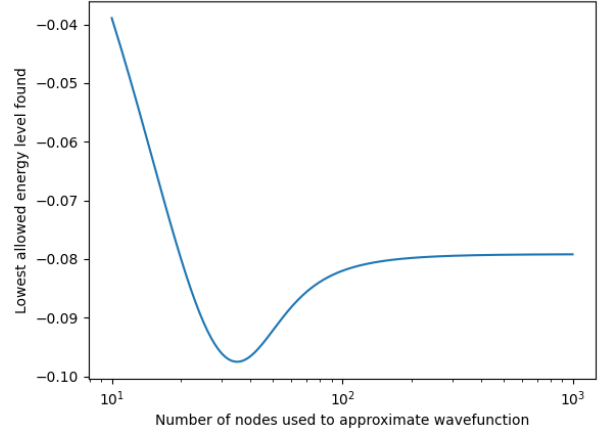

FIG. 3. The more nodes used to approximate the wavefunction, the better the approximation becomes. This plot depicts the calculated 2p energy level with $\delta = 0.025$ as a function of the number of nodes used to approximate the wavefunction. The value logarithmically approaches the true value as the number of nodes becomes very large. Note the logarithmic scale of the x axis.

IV. ANALYSIS

The energies computed in this work (Tab. I, column 3) show strong agreement with the numerical results of Varshni [5] (column 4) for lower orbitals (2p, 3p, 3d) and for lower screening parameters ($\delta \leq 0.15$). The discrepancies are typically on the order of 10^{-6} to 10^{-5} atomic units, demonstrating that the method employed here provides a highly accurate approximation in these cases. However, we can see that as both the orbital number (n) and δ increase, the agreement deteriorates. For

TABLE II. Uncertainties in radius and momentum calculated for successive energy levels of the $\ell = 1$ orbital. Assumes $\hbar = 1$.

Orbital	Δr	Δp	$\Delta r \Delta p$
2p	4.485	0.193	0.866
3p	9.816	0.136	1.338
4p	16.731	0.107	1.782
5p	22.611	0.113	2.562

instance, at $\delta = 0.35$ in the 2p state, the discrepancy grows to $\sim 10^{-4}$, while for higher orbitals (e.g., 5p, 6p at $\delta = 0.025$), this disagreement escalates to 10^{-3}–10^{-2} atomic units. This suggests that the approximation becomes less reliable for weakly bound (high-n) energy states or more strongly screened ($\delta \geq 0.2$) systems.

Next, we discuss the uncertainties reported in Tab. II. We observe that the uncertainty in position, Δr, increases as the principal quantum number increases. This trend aligns with the fact that lower energy levels are closer to the center of the radial potential and are thus more localized near the minimum of the potential well.

We can further understand this behavior by considering the effect of moving away from the potential minimum. As the particle's energy increases, its binding energy to the well decreases; therefore, higher energy levels correspond to orbitals with probability densities concentrated at larger radii. This is consistent with the expected behavior of a physical system governed by a radial potential.

Regarding the uncertainty in momentum (Δp), we can analyze the results from both a quantum and a somewhat classical perspective.

From the quantum perspective, the observed trend matches the predictions of the Heisenberg uncertainty principle, expressed as:

$$\Delta x \cdot \Delta p \gtrsim \hbar/2.$$

Although the principle is written in terms of Δx, the product $\Delta r \cdot \Delta p$ is proportional to this inequality. As the energy level increases, Δr increases, while Δp decreases, and vice versa.

Now, classically, consider a potential that is bound at a minimum and increases asymptotically as $r \rightarrow \infty$. At higher energies, states are less tightly confined, meaning the particle spends more time at larger distances where the potential is weaker. This results in a decrease in Δp at greater radii.

The data in Fig. 2 reveal a clear trend: as the screening parameter δ increases, the number of allowed energy levels decreases. We can consider this behavior as consistent with the physical interpretation of δ in the Hulthen potential, where larger δ values correspond to stronger screening of the Coulomb-like interaction. This reduc-

tion in the number of bound states at larger screening parameters happens because screening weakens the effective potential depth, reducing its ability to confine particles. At higher δ, the potential well becomes too shallow, and occurs at too small radii, to allow for as many higher-energy bound states.

We know that the nodal discretization directly impacts the solution accuracy because each node represents a point where the Schrödinger equation is approximated using finite differences. Thus the node density across the solved radius interval determines how well the wavefunction's spatial variations (particularly near potential minima) are captured. This constitutes the motivation behind creating Fig. 3. From this figure, we see that for $N > 100$ nodes, the lowest allowed energy asymptotically approaches its true value, with diminishing returns at higher node counts. For very few nodes ($N \ll 20$), the large spacing between grid points leads to numerical errors so large that the wavefunction curvature cannot be properly resolved, which explains the large error in these solutions.

V. CONCLUSION

This paper thus has successfully implemented a finite-difference method to solve the Schrödinger equation for the Hulthén potential, reproducing literature results with high accuracy ($\sim 10^{-6}$ a.u.) for low-lying states ($n \leq 4$) and moderate screening ($\delta \leq 0.15$). The method also yielded uncertainties that allowed for interpretations that match key quantum features: Δr increased with energy level due to reduced binding, Δp followed complementary behavior per the uncertainty principle, and screening effects reduced bound state counts as predicted. However, limitations emerged for high-n states ($n \geq 5$) and strong screening ($\delta \geq 0.2$), where errors grew to 10^{-3}–10^{-2} a.u., reflecting numerical instabilities in resolving weakly bound states.

Future work should focus on solving this method with an additional implementation of adaptive node placement to improve high-n state accuracy. Another avenue to building on the findings of this paper is the extension to time-dependent systems to model dynamic screening effects in relevant real-world systems such as plasma.

[1] Bhoi, J. and Laha, U. (2013). Hamiltonian hierarchy and n–p scattering. *Journal of Physics G: Nuclear and Particle Physics*, 40(4):045107.

[2] Jia, C.-S., Wang, J.-Y., He, S., and Sun, L.-T. (2000). Shape invariance and the supersymmetry wkb approximation for a diatomic molecule potential. *Journal of Physics A: Mathematical and General*, 33(39):6993–6998.

[3] Patil, S. H. (2001). Simple wavefunctions for Yukawa- and Hulthén-type potentials. *Journal of Physics A Mathematical General*, 34(14):3153–3167.

[4] Roy, A. K. (2015). Spherical confinement of coulombic systems inside an impenetrable box: H atom and the hulthén potential. *International Journal of Quantum Chemistry*, 115(15):937–947.

[5] Varshni, Y. P. (1990). Eigenenergies and oscillator strengths for the Hulthén potential. *Phys. Rev. A*, 41(9):4682–4689.